The Journal of the Acoustical Society of America

FEBRUARY 02 2026

Empirical correction method for spatial averaging effect in ultrasonic device calibration: Enhancing the precision-sensitivity trade-off

Francisco Alves; Mário Santos; André Alvarenga; Lorena Petrella

J. Acoust. Soc. Am. 159, 1027–1035 (2026)
https://doi.org/10.1121/10.0042356

JASA ARTICLE

Empirical correction method for spatial averaging effect in ultrasonic device calibration: Enhancing the precision-sensitivity trade-off

Francisco Alves,[1] Mário Santos,[1,2] André Alvarenga,[3] and Lorena Petrella[4,a)]

[1]University of Coimbra, Department of Electrical and Computer Engineering, Coimbra, Coimbra 3030-790, Portugal

[2]University of Coimbra, ARISE, CEMMPRE, Department of Electrical and Computer Engineering, Coimbra, Coimbra 3030-790, Portugal

[3]Medical, Marine and Nuclear Department, National Physical Laboratory, Hampton Road, Teddington, TW110LW, United Kingdom

[4]University of Coimbra, CISUC/LASI - Centre for Informatics and Systems of the University of Coimbra, Department of Informatics Engineering, Coimbra, Coimbra 3030-790, Portugal

ABSTRACT:
The calibration of ultrasound diagnostic equipment is essential to ensure their effectiveness and safety. Calibrating acoustic fields using hydrophones involves the measurement of the maximum pressure point. Since the signal at the hydrophone output is proportional to the average pressure incident on its surface, when the active area of the hydrophone is larger than the area of the ultrasonic beam at the focus, the lower acoustic pressures surrounding the point of maximum pressure will cause an underestimation of this value. This phenomenon is referred as the spatial averaging effect. The main limitation in the use of smaller hydrophones is the inherent reduction in sensitivity. The International Electrotechnical Commission standards provide methods to correct for the spatial averaging effect when the ratio of the – 6 dB beam width to the hydrophone diameter (R_{bh}) is higher than 1.5. In this study, a novel method is presented for spatial averaging correction, developed using computational simulation. It consists of an empirical correction factor and allows extending corrections for R_{bh} values as low as 0.35, with errors below 3%, addressing the compromise between precision and sensitivity of the hydrophone. This method also generalizes to ultrasonic probes with varying characteristics.
 https://doi.org/10.1121/10.0042356

(Received 19 July 2025; revised 3 January 2026; accepted 9 January 2026; published online 2 February 2026)

[Editor: Libertario Demi] Pages: 1027–1035

I. INTRODUCTION

The field of biomedical acoustics encompasses a wide range of diagnostic, therapeutic, and surgical applications. In all these applications, it is essential to accurately characterize the acoustic output to assess the safety and efficacy of medical procedures, ensuring compliance with regulatory requirements.[1,2] International standards and technical specifications describe relevant acoustic measurements for characterizing medical devices based on ultrasound.[1,3]

Acoustic field calibration involves the measurement of some main parameters, such as maximum compression acoustic pressures (p_c), maximum rarefaction acoustic pressures (p_r), and the pulse pressure squared integral (ppsi), which is the integral of the squared of the instantaneous acoustic pressure integrated over the acoustic pulse waveforms. These parameters are used to calculate acoustic exposure safety indices, such as the Mechanical Index and the Thermal Index for Soft Tissues, which provide an assessment of cavitation and heating effects produced by the exposure of biological tissue to ultrasonic energy.[4]

However, when the active area of the sensor element used in the calibration process is not sufficiently small compared to the dimensions of the -6 dB beam width at the focal plane (BW_{-6dB}) of the ultrasonic beam, the parameters are underestimated due to the spatial averaging effect.[1,4] Spatial averaging occurs when the sensor element measures not only the maximum pressure, but also the surrounding lower-pressure regions. The output of the sensor element will be proportional to the average incident pressure across its entire surface, thus underestimating the maximum pressure value.

A. Hydrophone dimensions

Ideally, the hydrophone diameter (d) should be smaller than the BW_{-6dB} [Fig. 1(a)]. Although, in most practical cases, the hydrophone diameters are larger than the ideal one [Fig. 1(b)], incurring in the spatial averaging effect. According to Ref. 4, the choice of the hydrophone radius for a specific application should bring into account the following considerations:

(i) The hydrophone radius should be smaller than or equal to one-quarter of the wavelength (λ), so that variations in

[a)]Email: lorenapetrella@dei.uc.pt

https://doi.org/10.1121/10.0042356

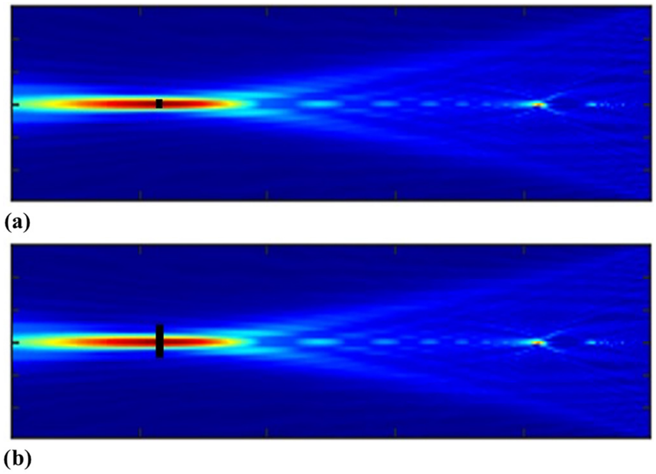

FIG. 1. Representation of an ultrasonic field with (a) a sensor diameter less than $2\,a_{max}$ and (b) a sensor whose diameter is greater than the diameter of the ultrasonic beam. The black markers represent the sensor surfaces. a_{max}, maximum recommended hydrophone radius.

the phase and amplitude of the wave do not significantly contribute to measurement uncertainties.

(ii) If it is not possible to meet the ideal condition, the maximum radius of the hydrophone (a_{max}) should be

$$a_{max} = \frac{\lambda}{8R}\left(F^2 + R^2\right)^{1/2}, \tag{1}$$

where R is the radius of the ultrasonic transducer and F is the focal length.

(iii) In cases where any of these criteria are met, it is recommended to compare the pressure values measured at the beam focus (maximum pressure) and at a radial distance equivalent to one hydrophone radius. If the decrease in the maximum signal amplitude at one radius away is greater than 1 dB, then the spatial averaging effect is significant, and corrections should be applied.[4]

B. Standard methods for spatial averaging effect correction

Some methods had been defined to correct the spatial averaging effect. Preston *et al.*[5] proposed (under some assumptions) a theoretical model using a correction factor (K_{sa}) for linear [Eq. (2)] and nonlinear [Eq. (3)] waves propagation,

$$K_{sa} = (3 - \beta)/2 \tag{2}$$

$$K'_{sa} = \left(3 - 2\beta'\right), \tag{3}$$

The parameters β and β' are defined by

$$\beta = \frac{\textit{signal at one hydrophone radius from axis}}{\textit{signal on the axis}}, \tag{4}$$

$$\beta' = \frac{\textit{signal at half hydrophone radius from axis}}{\textit{signal on the axis}}. \tag{5}$$

Smith[6] extended the study, introducing experimental approaches. Surprisingly, the experimental results showed a considerable disagreement with the predictions of the theoretical models, where the error of using hydrophones with diameters much larger than twice the maximum recommended radius [Eq. (1)] could lead to underestimations three times greater than those predicted by the theoretical methods. In that study, it was concluded that the factor that most influences this underestimation is the residual presence of nonlinear distortion, σ_m.[4–7] To quantify this effect, the nonlinear distortion parameter was defined as[4,8]

$$\sigma_m = \frac{\omega \cdot \beta_m \cdot z}{\rho \cdot c^3} p_m \frac{\ln\left(\left(F_g - 1\right)^{1/2} + {F_g}^{1/2}\right)}{\left(F_g - 1\right)^{1/2}}, \tag{6}$$

where β_m is the nonlinearity parameter (3.5 for pure water at 20° C), ω is the angular frequency, z is the distance between the surface of the probe and the plane of the wavefront, ρ is the medium density, c is the velocity of sound in the medium, p_m is the mean peak sound pressure (mean between $\mathrm{p_c}$ and $\mathrm{p_r}$) and F_g is 0.69 times the ratio of the geometric area of the probe to the area of the beam at −6 dB. Based on this parameter, the following rules are defined:[4,8]

(i) If $\sigma_m < 0.5$. Occurrence of little nonlinear distortion.

(ii) If $0.5 < \sigma_m < 1.5$. Considerable occurrence of nonlinear distortion; however, little attenuation occurs at pressure peaks.

(iii) If $\sigma_m > 1.5$. Considerable occurrence of nonlinear distortion and attenuation at pressure peaks.

The International Electrotechnical Commission (IEC) 62127-1:2022 standard, Annex E.1, establishes a method for correcting the spatial averaging effect based on the studies of Preston *et al.*[5] and Smith,[6] with some reservations. Here, it is considered that the process for correcting the spatial averaging effect, given by Eq. (2), provides reasonable estimates for $\sigma_m < 0.5$ and with associated uncertainties between 10% and 15%.[7] For more distorted waveforms, the standard provides some rules in terms of σ_m and the parameter R_{bh}, defined as[4]

$$R_{bh} = \frac{BW_{-6dB}}{d}, \tag{7}$$

where BW_{-6dB} can be obtained by Eq. (8), with f being the fundamental frequency and D being the transducer diameter.[9]

$$BW_{-6dB} = \frac{cF}{fD}. \tag{8}$$

(i) If $R_{bh} > 2$. For $0.5 < \sigma_m < 1.5$, the maximum correction for $\mathrm{p_c}$ and $\mathrm{p_r}$ is approximately 13% and for ppsi less than 25%. For $\sigma_m > 1.5$, corrections for $\mathrm{p_c}$ and $\mathrm{p_r}$ should not exceed 20%.

(ii) If $1.5 \le R_{bh} \le 2$. For $\sigma_m < 1.5$, the correction for $\mathrm{p_c}$ and $\mathrm{p_r}$ shall be less than 20% and the correction for ppsi shall not exceed 40%. For $\sigma_m > 1.5$, corrections

https://doi.org/10.1121/10.0042356

for p_c, p_r, and ppsi may be greater than 30%, 20%, and 50%, respectively.

(iii) If $R_{bh} < 1.5$. In these circumstances, for all values of σ_m, the corrections for p_r can be as high as 50%. On the other hand, the corrections for p_c can be in the order of 100% for $0.5 < \sigma_m < 1.5$, and up to 200% for $\sigma_m > 2$. Corrections for ppsi can reach 300%. Therefore, in situations where $R_{bh} < 1.5$, it is advisable to use a hydrophone with a smaller diameter.[4,7]

Subsequently, Wear and Liu[10] developed the inverse spectral filtering approach for the correction of the spatial averaging effect for linear and nonlinear beams propagation containing multiple harmonics. Some advantages of this approach are that it gives appropriate corrections at harmonic frequencies for nonlinear distorted waveforms, does not require a second measurement at one hydrophone radius from the axis, and can be applied to transducers with rectangular geometry.[10–13] For beams whose harmonics exhibit Gaussian profiles over the extent of the receiving area of the hydrophone, is defined a spatial averaging filter by[10]

$$S(nf) = \frac{1 - \exp\left(-\Omega_n{}^2\right)}{\Omega_n{}^2}, \tag{9}$$

where n is the harmonic number and Ω_n^2 is defined as

$$\Omega_n{}^2 = \frac{a^2(nf)}{2\sigma_n{}^2}, \tag{10}$$

$a(nf)$ being the frequency-dependent hydrophone radius and σ_n being the harmonic beam width. Equation (9) can be interpolated to frequencies between harmonics to generate filters with appropriated frequency resolution. The reciprocal of Eq. (9) is the spatial averaging correction factor to be applied to the measured pressure values. This method was adopted in the IEC 62127-1:2022 standard, Annex E.2, that extends to cases of nonlinear propagation.

Despite the standard methods for correcting spatial averaging effect, limitations can emerge in the calibration of highly focused ultrasonic beams, where hydrophones with sufficiently small diameters may exhibit reduced sensitivity. The new method proposed in this study addressed these situations, making corrections extensive to lower R_{bh} values.

II. MATERIALS AND METHODS

The k-Wave MATLAB toolbox (MathWorks, Inc., Natick, MA)[14] can be used to model and simulate wave propagation in different media, with a range of built-in features and functions that allow users to set up and run simulations efficiently. The suitability of this toolbox in the simulation of acoustic waves propagation under diverse conditions had been demonstrated in several studies. It consists of a numerical model for solving three coupled first-order partial differential equations, using a **k**-space pseudospectral method for the calculus of spatial and temporal gradients.[15] Moreover, the model accounts for power law acoustic absorption, using a linear integrodifferential operator.[16] Some of the key features of the k-Wave toolbox include support for one-dimensional (1D), two-dimensional (2D), and three-dimensional (3D) simulations, a variety of different input and output transducer configurations, and advanced visualization tools for analysing and interpreting simulation results.

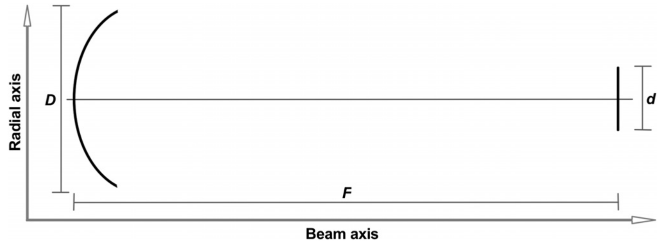

FIG. 2. 2D representation of the 3D simulations carried out using the k-Wave MATLAB toolbox. On the left side is the probe (source) with diameter D, and on the right side is the hydrophone (sensor), with diameter d. F is the focal length of the probe, which corresponds to the distance between source and sensor.

The simulations performed in the k-Wave toolbox, in the context of this study, were implemented in 3D and are schematically represented by the 2D illustration in Fig. 2. In this scheme, the source profile corresponds to a focused ultrasonic transducer with diameter D, the sensor represents a hydrophone with diameter d, and the distance between them is F, with water serving as the coupling medium. These dimensions vary for each specific configuration, whereas some parameters common to all the simulations are presented in Table I.[4,17,18]

The emitted pulse configuration was defined to reproduce that used in experimental measurements for a single probe[19] and extended to the remaining simulations to facilitate comparison. The signals captured by each grid element on the sensor surface were averaged at each time point to obtain the resultant pressure signal, accounting for the spatial averaging effect.

Since in practical calibration procedures the noise levels of the collected signals are commonly minimized using approaches like signals averaging and filtering, noise components were not introduced in the simulated signals.

In the present work, the simulations were carried out with an optimized GPU code that allows a considerable reduction in execution time, using a GeForce GTX 1080 Ti card (NVIDIA Corp., Santa Clara, CA), with a memory size of 11 GB.

TABLE I. Description and values of parameters used for defining the excitation pulse and propagation media, common to all simulations.

Description	Value (unit)
Peak amplitude of the emitted pulse	100 (kPa)
Number of cycles per burst	5
Attenuation coefficient of water	0.0022 [dB/(MHz^{2}cm)]
Power law absorption exponent of water	2
Density of water	997.3 (kg/m^3)
Sound velocity of water	1494 (m/s)
Material nonlinearity	5

A. Preliminary tests

Two methods were tested for source and sensor representations: one using the makeBowl function, with the structure depicted in Fig. 3(a); another using the kWaveArray function, illustrated in Fig. 3(b).[14,20] This second function applies weights to each point of the grid that constitutes the represented element, with elements near the border having weights close to zero, reducing the stair-case geometry effect.[14,20]

The two methods were evaluated by comparison of the gain in focal pressure, with the expected theoretical value (G), given by[21]

$$G = \frac{k \times R^2}{2F}, \tag{11}$$

where k is the wave number. The root mean squared error (RMSE) of G for the makeBowl and KWaveArray functions were 1.2374 and 0.3326, respectively. Being so, the second approach was used throughout the study.

In a second phase, it was studied how the resolution of the computational grid affects the pressure signal measured in the sensor. The resolution (dx), which is the voxel size, in turn defines the number of points per wavelength (ppw), and they are related by Eq. (12),

$$dx = \frac{c}{ppw \times f}. \tag{12}$$

Tests were conducted with ppw values ranging from three (minimum value for homogeneous media[14]) up to the maximum ppw supported by the GPU for each simulated probe. While tests conducted for probe A using different ppw values evidenced low root mean squared percentual errors (RMSPEs) of 1.2%, 0.8%, and 0.9% for the p_c, $p_{r,}$ and ppsi parameters, respectively, the best possible grid resolution was used throughout the study.

B. Simulations setup

The probe/sensor configurations experimentally tested by Smith,[6] covering a wide range of ultrasonic medical equipment, were used as reference for the simulations implemented in this work. The most relevant characteristics of the transducers are presented in Table II (probes A, B, and C). In addition, the configuration of probe D was included, representing a transducer used in our previous studies.[19,22] Probes A, B, and C were used in the development of the empirical model, whereas probe D was used to evaluate the feasibility of extending the method to probes with different characteristics.

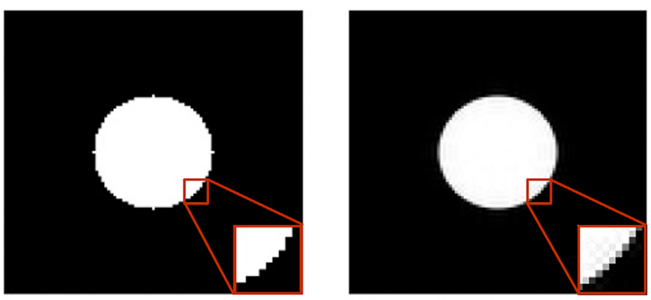

FIG. 3. 2D representation of the 3D disk using (a) the makeBowl function and (b) the kWaveArray function. (b) Weights are applied to the grid units to reduce the stair-case geometry effect.

TABLE II. Transducer configurations considered for simulations.

Probes	Frequency (MHz)	Transducer radius (mm)	Focal length (mm)
A	10	3.1	20
B	5	6.5	55
C	3.5	6.5	55
D	20	1.6	9

Diverse hydrophone diameters were considered, including hydrophones with 1, 0.5, 0.2, and 0.1 mm in diameter. Also, point hydrophones with size equal to the grid resolution (on the order of few tens of micrometers) were used as reference, as well as hydrophones with diameters equal to BW_{-6dB} [Eq. (8)]. Further hydrophones configurations were simulated to evaluate the extendibility of the proposed approach. Hydrophones diameters ranging from the maximum recommended value ($2 \cdot a_{max}$) up to $22 \cdot a_{max}$ were simulated. The diameters were progressively increased in steps equal to the voxel size.

C. Application of the corrections given by IEC 62127-1: 2022

The parameters p_c, $p_{r,}$ and ppsi were obtained from the simulated signals, collected at the focus of the ultrasonic beam, and at a radial distance equal to one hydrophone radius. Then, the two standard correction methods given by Eqs. (2) and (9) were applied.

D. Novel correction method

The first step was to depict the relationship between R_{bh}[6] and the p_c, $p_{r,}$ and ppsi values. On this sense, the normalized pressure values were represented as function of R_{bh}. Then, the new correction factor (K) is estimated as the ratio of the pressure value measured by a pointwise hydrophone (P) and the pressure (P_i) measured by a hydrophone of arbitrary diameter [Eq. (13)],

$$K = \frac{\mathrm{P}}{P_i}. \tag{13}$$

The next step is to find a curve function that best fits the K values as function of R_{bh}. On this sense, regression was applied to three predefined models, including exponential [Eq. (14)], power [Eq. (15)], and rational [ratio between polynomials, Eq. (16)], using MATLAB R2023a. In these equations, a_i, b_i, p_i, and q_j are the model coefficients to be estimated, with $i = 1, 2, 3$ and $j = 1, 2$,

$$K_{\exp} = a_1 + a_2\, e^{-a_3 R_{bh}}, \tag{14}$$

$$K_{pow} = b_1 + b_2 R_{bh}^{\;b_3}, \tag{15}$$

$$K_{rp} = \frac{p_1 R_{bh}^{\;2} + p_2 R_{bh} + p_3}{R_{bh}^{\;2} + q_1 R_{bh} + q_2}. \tag{16}$$

III. RESULTS

Table III presents the ppw, dx, $a_{max,}$ and BW_{-6dB} values for each simulated probe.

A. Visualization of the spatial averaging effect

Figure 4 shows the pressure values calculated along a radial line in the focal plane of probe A, for different hydrophone diameters. A significant reduction in the maximum values of p_c, p_r, and ppsi are observed, when using larger hydrophones evidencing the spatial averaging effects.

B. Corrections by IEC 62127-1: 2022 methods

To compare the correction factor given by the IEC 62127-1:2022 with the proposed approach, the parameter σ_m [Eq. (6)] was first calculated for the different probes, obtaining the values presented in Table III. Since all values are less than 0.5, we can conclude that there is small nonlinear distortion, so this effect can be neglected.

Figure 5 presents the corrected pressure values using the two approaches proposed in the IEC 62127-1:2022 standard (Annex E.1 and E.2), presented in Eqs. (2) and (9). The inverse spectral filtering approach was implemented only for p_c and p_r parameters since the correction of ppsi using this method has not been documented.

From Fig. 5, it is observed that for the method proposed in IEC 62127-1:2022, Annex E.1, when R_{bh} is greater than 1.5 (hydrophone diameter smaller than 0.14 mm), the corrected values of p_c, $p_{r,}$ and ppsi present results very close to those measured by a pointwise hydrophone. However, when using hydrophones with larger diameters, the differences between the corrected pressure values and those measured by a pointwise hydrophone increase (the corrected values decrease), highlighting the limitations of the correction method in such cases, where it is no longer appropriated to compensate for the spatial averaging effect. The inverse spectral filtering approach, from IEC 62127-1:2022 Annex E.2, presents better results than the previous method,[10,11] closely approximating to values measured by a pointwise hydrophone for hydrophones with R_{bh} of about one; however, for larger hydrophones, the errors increase.

TABLE III. Points per wavelength (ppw), grid resolution (dx), maximum hydrophone radius (a_{max}), -6 dB beam width at the focal plane (BW_{-6dB}), and nonlinear distortion parameter (σ_m) for the different simulated probes.

Probes	ppw	dx (μm)	a_{max} (μm)	BW_{-6dB} (μm)	σ_m
A	6	24.9	60.96	481.9	0.34
B	5	59.8	159.1	1264.2	0.44
C	7	61.0	227.3	1805.9	0.27
D	6	12.5	26.67	210.1	0.31

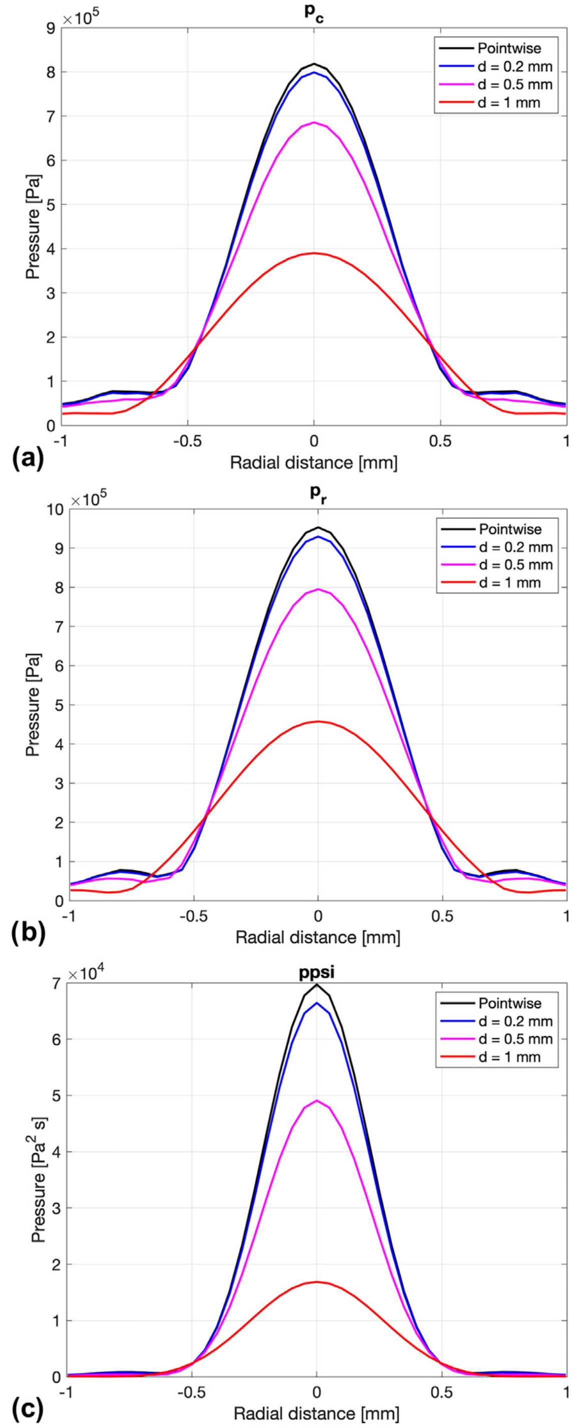

FIG. 4. Pressure values obtained for different hydrophone diameters (d), for probe A. The values of (a) p_c, (b) p_r, and (c) ppsi are shown for hydrophones with diameters of 24.9 μm (pointwise) and 0.2, 0.5, and 1 mm. The pressure curves were obtained from the average pressure at the grid points corresponding to the different hydrophone positions and sizes along the radial direction in the focal plane. p_c, maximum compression acoustic pressure; p_r, maximum rarefaction acoustic pressure; ppsi, pulse pressure squared integral.

C. New method for correction of the spatial averaging effect

It was possible to verify that the normalized p_c and p_r values vary in a very similar way as a function of R_{bh} (Fig. 6), which is expected in the absence of nonlinear

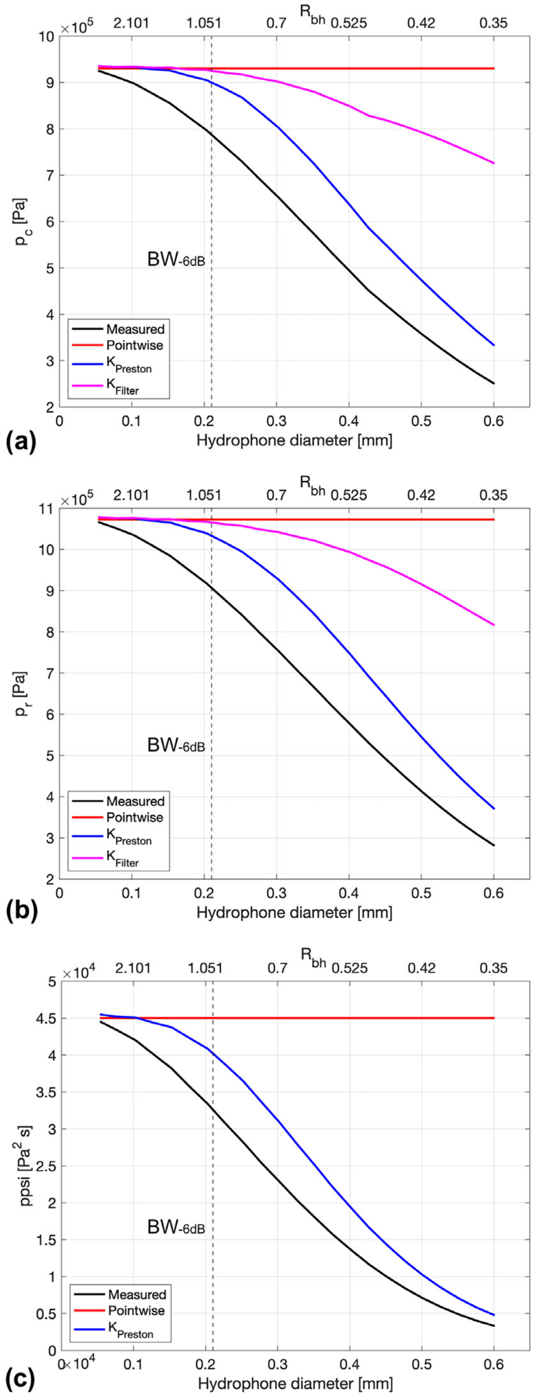

FIG. 5. Maximum pressure values of (a) p_c, (b) p_r, and (c) ppsi as a function of the hydrophone diameters (bottom axis) and the R_{bh} parameter (top axis), for probe D. Black curve: pressure values without spatial averaging correction; blue curves: pressure values corrected by K_{sa} factor ($K_{Preston}$); magenta curves: pressure values applying the inverse spectral filtering approach (K_{Filter}); red curves: pressure values measured by a pointwise hydrophone; dashed line: representation of the -6 dB beam width (BW_{-6dB}). Note that the highest hydrophone diameter corresponds to a ratio of hydrophone diameter to wavelength of eight. p_c, maximum compression acoustic pressure; p_r, maximum rarefaction acoustic pressure; ppsi, pulse pressure squared integral.

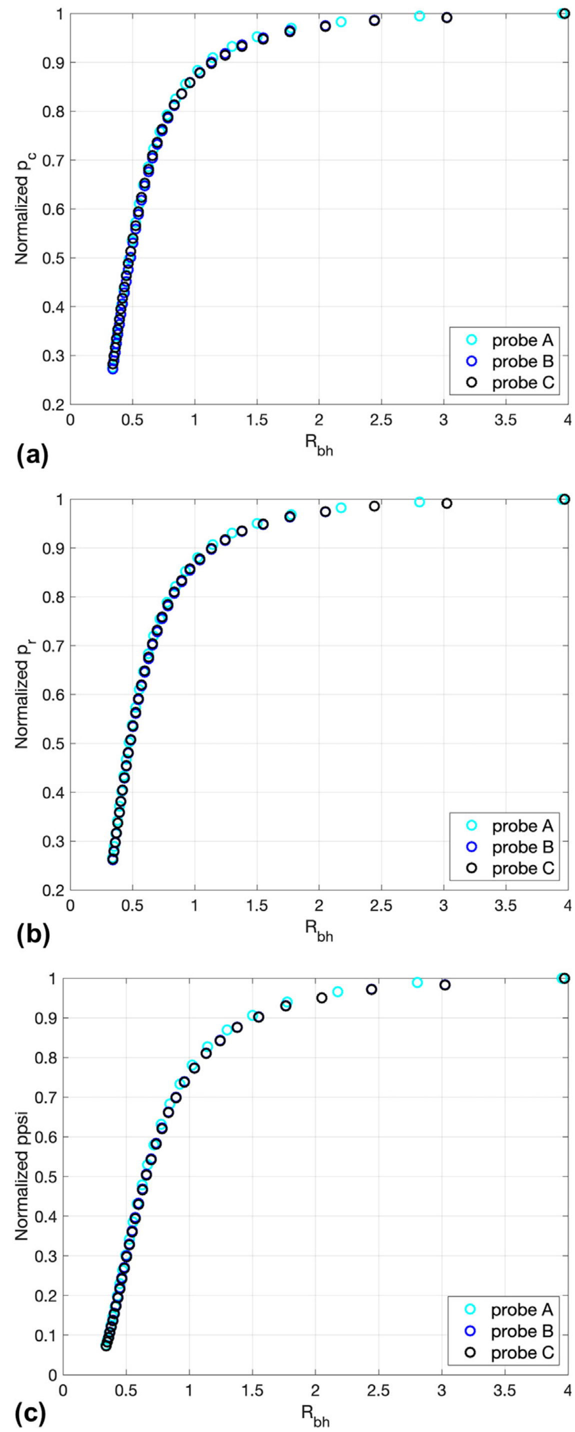

FIG. 6. Normalized pressure values of (a) p_c, (b) p_r, and (c) ppsi as a function of R_{bh}. A, B, and C refer to the different simulated probes. Note that the p_c and p_r normalized pressures follow the same distribution. p_c, maximum compression acoustic pressure; p_r, maximum rarefaction acoustic pressure; ppsi, pulse pressure squared integral.

distortion, whereas ppsi inherently yields lower values. It is also observed that the normalized pressures follow the same profile for the three simulated probes. Based on these observations, two correction factors were determined, the K_p for p_c and p_r, and the K_{ppsi} for ppsi. Figure 7 presents the results as a function of R_{bh}.

D. Regression of the correction factors

The values obtained for K_p and K_{ppsi} (including all combinations of hydrophones and probes, Fig. 7) were fitted to

https://doi.org/10.1121/10.0042356

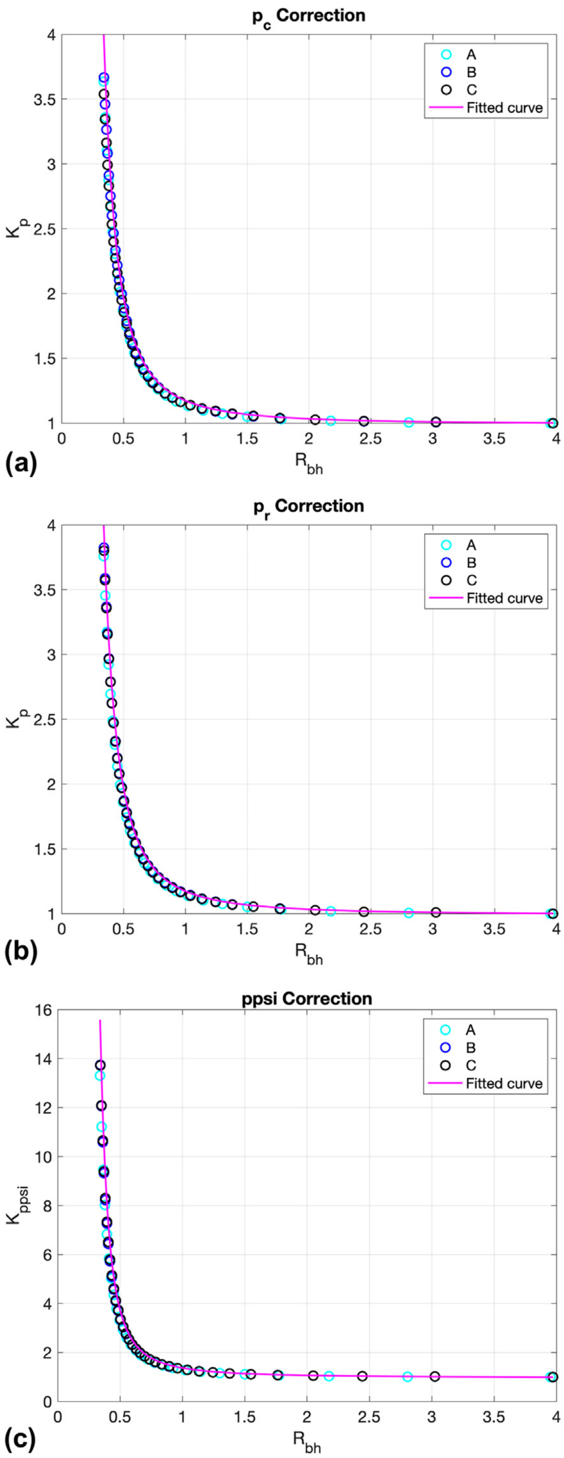

FIG. 7. Correction factors and fitted curves based on a ratio between polynomials, represented as a function of R_{bh} for (a) p_c, (b) p_r, and (c) ppsi. A, B, and C refer to the different simulated probes. The fitted curves for p_c and p_r follow the same equation. p_c, maximum compression acoustic pressure; p_r, maximum rarefaction acoustic pressure; ppsi, pulse pressure squared integral.

the models described by Eqs. (14)–(16). The results obtained for the exponential curve, the power curve, and to the ratio between polynomials are presented in Eqs. (17)–(19), respectively,

$$K_p = 1.0839 + 22.4095e^{-6.4661R_{bh}}, \tag{17a}$$

TABLE IV. Maximum positive and negative errors, and RMSE, between real and corrected pressure values, and for each approximation, applied to probe D. p_c, maximum compression acoustic pressure; p_r, maximum rarefaction acoustic pressure; ppsi, pulse pressure squared integral.

Approximation	Parameter	Maximum positive error (%)	Maximum negative error (%)	RMSE
Exponential	p_c	7.8	8.2	44.8 kPa
	p_r	7.7	10.4	53.8 kPa
	ppsi	39.6	18.9	7.7 kPa^{2}s
Power	p_c	3.2	2.7	16.0 kPa
	p_r	3.1	2.6	17.2 kPa
	ppsi	22.9	9.9	4.1 kPa^{2}s
Rational	p_c	0.7	2.3	9.2 kPa
	p_r	0	1.8	8.5 kPa
	ppsi	1.7	1.7	0.5 kPa^{2}s

$$K_{ppsi} = 1.4113 + 729.3394e^{-11.7390R_{bh}}, \tag{17b}$$

$$K_p = 1.0351 + 0.1222R_{bh}{}^{-2.9443}, \tag{18a}$$

$$K_{ppsi} = 1.2146 + 0.1005R_{bh}{}^{-4.5759}, \tag{18b}$$

$$K_p = \frac{0.9890R_{bh}{}^2 - 0.2723R_{bh} + 0.1428}{R_{bh}{}^2 - 0.2920R_{bh} + 0.0248}, \tag{19a}$$

$$K_{ppsi} = \frac{0.9517R_{bh}{}^2 - 0.3771R_{bh} + 0.1843}{R_{bh}{}^2 - 0.5155R_{bh} + 0.0703}. \tag{19b}$$

The RMSPE of the fitted K_p curves were 4.2%, 5.2%, and 5.1% for the results obtained from Eqs. (17a), (18a), and (19a), respectively; the fitted K_{ppsi} curves have associated RMSPE of 18.8%, 11.1%, and 9.1%, following Eqs. (17b), (18b), and (19b), respectively. These equations were then used for correcting the pressure values as function of R_{bh}. Table IV presents the correction results for probe D, where the maximum positive error (due to overestimation), maximum negative error (due to underestimation), and the RMSE for p_c, p_r, and ppsi values for each of the implemented models are indicated. It is observed that the correction modeled as a ratio between polynomials presents the best results, as evidenced by the lowest RMSE across the three parameters (Table IV). The corrected measurements for this best model and for probe D are presented in Fig. 8. Here, it can be observed how the pressure values measured with hydrophone sizes that considerably exceed the ideal size can be compensated by the correction factor implemented and closely approximate to the measures obtained with a pointwise hydrophone.

IV. DISCUSSION AND CONCLUSION

The present study proposes a novel method, developed using computational simulations, for the correction of the spatial averaging effect in the calibration of ultrasonic fields. For defining the correction factor, the relationship between p_c, p_r, and ppsi with the parameter R_{bh} was approximated to

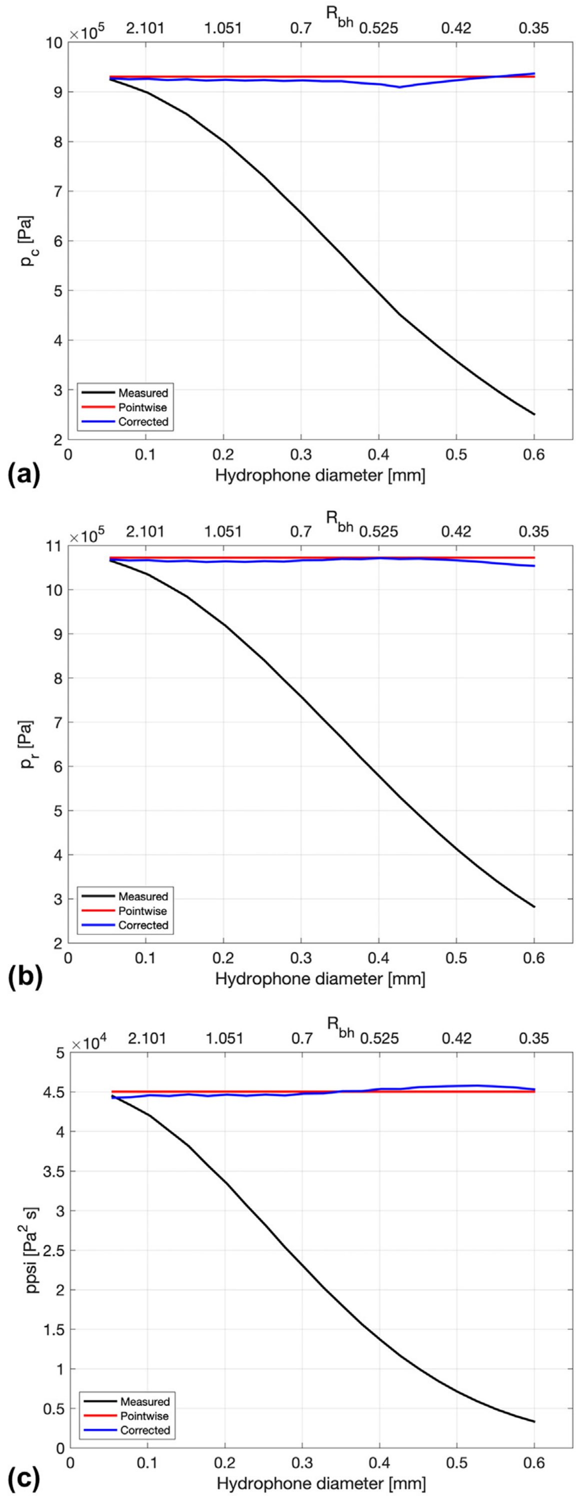

FIG. 8. Maximum pressure values of (a) p_c, (b) p_r, and (c) ppsi, with and without spatial averaging effect correction. Simulated results are presented as a function of the hydrophone diameter (bottom axis) and R_{bh} (top axis), for probe D. Black curves: pressure values without spatial averaging correction; blue curves: pressure values corrected by the new method; red curves: pressure values measured by a pointwise hydrophone. In this approach, the relationship K_p vs R_{bh} and K_{ppsi} vs R_{bh} was modeled by a ratio between polynomials. Note that the highest hydrophone diameter corresponds to a ratio of hydrophone diameter to wavelength of eight. p_c, maximum compression acoustic pressure; p_r, maximum rarefaction acoustic pressure; ppsi, pulse pressure squared integral.

three different models: an exponential curve [Eqs. (17a) and (17b)], a power curve [Eqs. (18a) and (18b)], and a ratio between polynomials [Eqs. (19a) and (19b)] being the correction errors presented in Table IV. From a safety point of view, in medical applications, it should be noted that the underestimation of the pressure values results in a more critical situation than when they are overestimated. In this sense, the errors obtained using the exponential approach represent the less favorable case. The corrections based on the power curve approximation present better results although there is still an underestimation of the pressure values, particularly evident for ppsi. On the other hand, the approximation using a ratio between polynomials presents the best results for all the evaluated parameters, with maximum errors not exceeding 3%.

The proposed method was compared with the two approaches presented in the IEC 62127-1:2022 standard, Annex E.[4] Whereas this method mimics well the correction proposed by the IEC standard for greater values of R_{bh}, it was also possible to extend the correction factor to situations where the hydrophone diameter considerably exceeds the maximum recommended size [Eq. (1)]. Indeed, a good performance for R_{bh} values as low as 0.35 was demonstrated, whereas the standard methods are only applicable to R_{bh} values higher than 1.5. Also, since the normalized p_c, p_r, and ppsi values showed a similar relation with R_{bh}, across all simulated probes, the adaptability of the developed method to diverse probe characteristics was evidenced. Finally, the application of the proposed correction is also a simple approach, not requiring additional measurements of the acoustic field.

The correction method developed in this study may represent a particularly valuable approach for the calibration of highly focused ultrasonic beams including both high-intensity focused ultrasound (HIFU) and high-frequency ultrasound, as each technique presents specific challenges for the precise measurements of the acoustic fields.[23] HIFU, with increasing therapeutic applications, is characterized by tightly focused acoustic fields (i.e., low BW_{-6dB}) requiring the use of hydrophones with very small effective diameters. This issue is exacerbated by the effective hydrophone dimensions commonly exceeding the nominal dimensions at frequencies of few megahertz typically employed in HIFU.[24–26] This discrepancy mainly arises from diffraction effects in needle hydrophones, and from Lamb-waves propagation in membrane hydrophones.[27] For example, at $\sim$1 MHz, the effective size has been shown to reach up to ten times the nominal size, while at $\sim$3 MHz, it can be four times larger, while the effective and nominal sizes converge at higher frequencies.[27] In this context, the ability to extend correction factors to low R_{bh} values offers clear advantages.

On the other hand, diagnostic applications of high-frequency ultrasound typically involve focused acoustic fields at frequencies between 20 and 100 MHz,[28,29] with BW_{-6dB} on the order of only a few tens of micrometres and so requiring very small sensors. Also, the low acoustic intensities inherent to this technique further exacerbate the hydrophone trade-off between resolution and sensitivity.

Once again, the consideration of lower R_{bh} values with the proposed correction method provides a practical solution for correcting spatial averaging effects.

In conclusion, a method for correcting the spatial averaging effect, based on computational simulations, with a main advantage of being extensible to cases of lower R_{bh} values, in comparison to standard methods, is proposed in this study. Other valuable characteristics of the proposed approach include its simplicity and the adaptability to ultrasonic probes with different characteristics (sizes, focal distances, and operating frequencies). Future approaches should include experimental measurements to corroborate our simulated results, which the authors were unable to conduct due to laboratorial constraints. In addition, extend the applications to cases of nonlinear distortion and evaluate the applicability to ultrasonic probes of different geometries should be considered.

ACKNOWLEDGMENTS

This work was supported by the national funds through FCT – Fundação para a Ciência e a Tecnologia (Project Nos. UIDB/00326/2025, UIDP/00326/2025, UIDB/00285/2020, and LA/P/0112/2020). The funding source was not involved in the study design, collection, analysis, and interpretation of data, writing of the report, and decision to submit the article for publication.

AUTHOR DECLARATIONS

Conflict of Interest

The authors have no conflicts to disclose.

DATA AVAILABILITY

The data that support the findings of this study are available from the corresponding author upon reasonable request.

[1]G. R. Harris, S. M. Howard, A. M. Hurrell, P. A. Lewin, M. E. Schafer, K. A. Wear, V. Wilkens, and B. Zeqiri, "Hydrophone measurements for biomedical ultrasound applications: A review," IEEE Trans. Ultrason. Ferroelectr. Freq. Control **70**, 85–100 (2023).

[2]H. Azhar, *Basics of Biomedical Ultrasound for Engineers*, 1st ed. (John Wiley & Son, Inc., Hoboken, NJ, 2010).

[3]Food and Drug Administration, "Marketing clearance of diagnostic ultrasound systems and transducers - Guidance for industry and food and drug administration staff," https://www.fda.gov/media/71100/download (Last viewed May 29, 2025).

[4]IEC 62127-1: *Ultrasonics - Hydrophones - Part 1: Measurement and characterization of medical ultrasonic fields up to 40 MHz* (International Electrotechnical Commission, Geneva, Switzerland, 2007).

[5]R. C. Preston, D. R. Bacon, and R. A. Smith, "Calibration of medical ultrasonic equipment-procedures and accuracy assessment," IEEE Trans. Ultrason. Ferroelectr. Freq. Control **35**, 110–121 (1988).

[6]R. A. Smith, "Are hydrophones of diameter 0.5 mm small enough to characterise diagnostic ultrasound equipment?," Phys. Med. Biol. **34**, 1593–1607 (1989).

[7]B. Zeqiri and A. D. Bond, "The influence of waveform distortion on hydrophone spatial-averaging corrections—Theory and measurement," J. Acoust. Soc. Am. **92**, 1809–1821 (1992).

[8]D. R. Bacon, "Finite amplitude distortion of the pulsed fields used in diagnostic ultrasound," Ultrasound Med. Biol. **10**, 189–195 (1984).

[9]S. Foster, G. R. Lockwood, L. K. Ryan, K. A. Harasiewicz, L. Berube, and A. M. Rauth, "Principles and applications of ultrasound backscatter microscopy," IEEE Trans. Ultrason. Ferroelectr. Freq. Control **40**, 608–617 (1993).

[10]K. A. Wear and Y. Liu, "Considerations for choosing sensitive element size for needle and fiber-optic hydrophones - Part II: Experimental validation of spatial averaging model," IEEE Trans. Ultrason. Ferroelectr. Freq. Control **66**, 340–347 (2019).

[11]K. A. Wear, "Considerations for choosing sensitive element size for needle and fiber-optic hydrophones - Part I: Spatiotemporal transfer function and graphical guide," IEEE Trans. Ultrason. Ferroelectr. Freq. Control **66**, 318–339 (2019).

[12]K. A. Wear, A. Shah, A. M. Ivory, and C. Baker, "Hydrophone spatial averaging correction for acoustic exposure measurements from arrays - Part II: Validation for ARFI and pulsed Doppler waveforms," IEEE Trans. Ultrason. Ferroelectr. Freq. Control **68**, 376–388 (2021).

[13]K. A. Wear, "Hydrophone spatial averaging correction for acoustic exposure measurements from arrays - Part I: Theory and impact on diagnostic safety indexes," IEEE Trans. Ultrason. Ferroelectr. Freq. Control **68**, 358–375 (2021).

[14]B. E. Treeby and B. T. Cox, "k-Wave: MATLAB toolbox for the simulation and reconstruction of photoacoustic wave fields," J. Biomed. Opt. **15**, 021314 (2010).

[15]B. E. Treeby, J. Jaros, A. P. Rendell, and B. T. Cox, "Modeling nonlinear ultrasound propagation in heterogeneous media with power law absorption using a *k*-space pseudospectral method," J. Acoust. Soc. Am. **131**, 4324–4336 (2012).

[16]B. E. Treeby and B. T. Cox, "Modeling power law absorption and dispersion for acoustic propagation using the fractional Laplacian," J. Acoust. Soc. Am. **127**, 2741–2748 (2010).

[17]M. O. Culjat, D. Goldenberg, P. Tewari, and R. S. Singh, "A review of tissue substitutes for ultrasound imaging," Ultrasound Med. Biol. **36**, 861–873 (2010).

[18]S. L. Garrett, *Understanding acoustics - An Experimentalist's View of Sound and Vibration*, 2nd ed. (Springer International Publishing AG, Cham, Switzerland, 2020).

[19]L. Petrella, C. Pinto, F. Perdigão, M. Gomes, M. Santos, S. Nunes, M. Morgado, M. Caixinha, and J. Santos, "A-scan ultrasonic system for real time automatic cataract detection," Health Technol. **10**, 905–911 (2020).

[20]E. S. Wise, B. T. Cox, J. Jaros, and B. E. Treeby, "Representing arbitrary acoustic source and sensor distributions in Fourier collocation methods," J. Acoust. Soc. Am. **146**, 278–288 (2019).

[21]O. V. Bessonova, V. A. Khokhlova, M. R. Bailey, M. S. Canney, and L. A. Crum, "Focusing of high power ultrasound beams and limiting values of shock wave parameters," Acoust. Phys. **55**, 463–473 (2009).

[22]L. Petrella, P. Fernandes, M. Santos, M. Caixinha, S. Nunes, C. Pinto, M. Morgado, J. Santos, F. Perdigão, and M. Gomes, "Safety assessment of an A-scan ultrasonic system for ophthalmic use," J. Ultrasound Med. **39**, 2143–2150 (2020).

[23]Y. Liu, K. A. Wear, and G. R. Harris, "Variation of high-intensity therapeutic ultrasound (HITU) pressure field characterization: Effects of hydrophone choice, nonlinearity, spatial averaging and complex deconvolution," Ultrasound Med. Biol. **43**, 2329–2342 (2017).

[24]W. Wang, Y. Wang, T. Wang, J. Wang, L. Wang, and J. Tang, "Safety and efficacy of US-guided high-intensity focused ultrasound for treatment of submucosal fibroids," Eur. Radiol. **22**, 2553–2558 (2012).

[25]P. Cabras, P. Auloge, F. Bing, P. P. Rao, S. Hoarau, E. Dumont, A. Durand, B. Maurin, B. Wach, L. Cuvillon, E. Breton, A. Gangi, and J. Vappou, "A new versatile MR-guided high-intensity focused ultrasound (HIFU) device for the treatment of musculoskeletal tumors," Sci. Rep. **12**, 1–11 (2022).

[26]D. Cranston, T. Leslie, and G. ter Haar, "A review of high-intensity focused ultrasound in urology," Cancers **13**, 1–9 (2021).

[27]E. Martin and B. Treeby, "Investigation of the repeatability and reproducibility of hydrophone measurements of medical ultrasound fields," J. Acoust. Soc. Am. **145**, 1270–1282 (2019).

[28]G. Mannino, B. Abdolrahimzadeh, S. Calafiore, G. Anselmi, C. Mannino, and A. Lambiase, "A review of the role of ultrasound biomicroscopy in glaucoma associated with rare diseases of the anterior segment," Clin. Ophthalmol. **10**, 1453–1459 (2016).

[29]J. Levy, D. L. Barrett, N. Harris, J. J. Jeong, X. Yang, and C. S. Chen, "High-frequency ultrasound in clinical dermatology: A review," Ultrasound J. **13**, 1–12 (2021).